International Journal of Neural Systems, Vol. 28, No. 7 (2018) 1850002 (19 pages)

DOI: 10.1142/S0129065718500028

Principal States of Dynamic Functional Connectivity Reveal the Link Between Resting-State and Task-State Brain: An fMRI Study

Lin Cheng
School of Biomedical Engineering, Shanghai Jiao Tong University
Shanghai 200030, P. R. China
School of Biomedical Engineering, Science & Health Systems
Drexel University, Philadelphia, Pennsylvania, USA
chenglinsjtu@gmail.com

Yang Zhu
Department of Neurology, Shanghai Second People's Hospital
Shanghai 200011, P. R. China
Zhuyang1114@sina.cn

Junfeng Sun* and Lifu Deng†
School of Biomedical Engineering, Shanghai Jiao Tong University
Shanghai 200030, P. R. China
**jfsun@sjtu.edu.cn*
†*turbinicarpus@sjtu.edu.cn*

Naying He
Department of Radiology, Rui Jin Hospital, School of Medicine
Shanghai Jiao Tong University
Shanghai 200025, P. R. China
i@nayinghe.com

Yang Yang
Department of Neurology, Shanghai Second People's Hospital
Shanghai 200011, P. R. China
yangy20008@163.com

Huawei Ling
Department of Radiology, Rui Jin Hospital, School of Medicine
Shanghai Jiao Tong University
Shanghai 200025, P. R. China
huaweiling1965@sina.com

Hasan Ayaz
School of Biomedical Engineering, Science & Health Systems
Drexel University, Philadelphia, Pennsylvania, USA
Hasan.ayaz@drexel.edu

Yi Fu‡
Department of Neurology & Institute of Neurology, Rui Jin Hospital
School of Medicine, Shanghai Jiao Tong University
Shanghai 200025, P. R. China
fuyiki@sina.com

‡Corresponding authors.

Shanbao Tong‡
School of Biomedical Engineering, Shanghai Jiao Tong University
Shanghai 200030, P. R. China
stong@sjtu.edu.cn

Accepted 8 January 2018
Published Online 2 April 2018

Task-related reorganization of functional connectivity (FC) has been widely investigated. Under classic static FC analysis, brain networks under task and rest have been demonstrated a general similarity. However, brain activity and cognitive process are believed to be dynamic and adaptive. Since static FC inherently ignores the distinct temporal patterns between rest and task, dynamic FC may be more a suitable technique to characterize the brain's dynamic and adaptive activities. In this study, we adopted k-means clustering to investigate task-related spatiotemporal reorganization of dynamic brain networks and hypothesized that dynamic FC would be able to reveal the link between resting-state and task-state brain organization, including broadly similar spatial patterns but distinct temporal patterns. In order to test this hypothesis, this study examined the dynamic FC in default-mode network (DMN) and motor-related network (MN) using Blood-Oxygenation-Level-Dependent (BOLD)-fMRI data from 26 healthy subjects during rest (REST) and a hand closing-and-opening (HCO) task. Two principal FC states in REST and one principal FC state in HCO were identified. The first principal FC state in REST was found similar to that in HCO, which appeared to represent intrinsic network architecture and validated the broadly similar spatial patterns between REST and HCO. However, the second FC principal state in REST with much shorter "dwell time" implied the transient functional relationship between DMN and MN during REST. In addition, a more frequent shifting between two principal FC states indicated that brain network dynamically maintained a "default mode" in the motor system during REST, whereas the presence of a single principal FC state and reduced FC variability implied a more temporally stable connectivity during HCO, validating the distinct temporal patterns between REST and HCO. Our results further demonstrated that dynamic FC analysis could offer unique insights in understanding how the brain reorganizes itself during rest and task states, and the ways in which the brain adaptively responds to the cognitive requirements of tasks.

Keywords: Dynamic functional connectivity; functional magnetic resonance imaging; functional connectivity state; k-means clustering; default-mode network; motor function.

1. Introduction

The resting-state brain is believed to operate under a "default mode" in the absence of specific cognitive demands, which is expected to be a state of readiness for upcoming tasks.[1–3] The understanding of how brain networks establish the "default mode" and reorganize spatiotemporally in response to tasks is critical for revealing the underlying adaptation within the brain during cognitive processes.[4–9] So far, several studies have examined the task-related modulation of brain networks, and reported a decrease of default-mode network (DMN) functional connectivity (FC) during externally oriented cognitive tasks,[10,11] and an increase of an inter-network FC between DMN and other task-related areas during internally oriented mental activities.[12,13] Although task-modulation of FC has been established, overall similarities in the spatial patterns of brain networks have been reported during rest and a variety of other tasks. This phenomena is often attributed to intrinsic network architectures present in both rest and tasks.[14–18] Nonetheless, FC in these studies was estimated using the whole time course under the assumption that the brain networks would be relatively stable during the recording process. However, this assumption may not be entirely justified as brain activities and cognitive processes are known to be dynamic and adaptive,[19,20] an observation that has been repeatedly confirmed by time–frequency analysis[21] as well as dynamic FC analysis.[22] Thus, investigation of the spatiotemporal modulation of dynamic brain networks during tasks may further help to understand the adaptation of brain to cognitive process requirements.[18,23–25]

Dynamic brain activities have been extensively studied using EEG methods and commonly observed functional microstates have been considered to form

the basic building blocks of information processing.[26–33] fMRI-based investigations using dynamic FC have been the focus of recent methodological innovations and studies are also accumulating.[23,24,34,35] Dynamic FC has been explored in fMRI using sliding window correlation analysis to examine time scales ranging from seconds to minutes.[21,36–38] These studies demonstrated that dynamic FC analysis not only delivers a more complete description of the temporal dependence of the brain's organization during cognitive processes, but also this perspective provides clinically valuable information. For example, schizophrenia patients exhibited shorter states of strong and large-scale FC than healthy controls during rest, which cannot be observed when using static FC analysis.[37] Another study of dynamic FC in Alzheimer's disease patients showed longer state persistence in the strong anterior DMN subnetwork, but shorter states in the strong posterior DMN sub-network when compared with healthy elderly subjects during rest.[38] For the cognitive process during rest, a recent resting-state dynamic FC study reported that multiple FC states could coexist, which was interpreted as an indication of the unconstrained mental activities of resting state,[36] an observation further supported by positive correlation between frequency of "mind-wandering" and FC variability (FCV) in core regions of interest (ROIs) in DMN.[39] In addition, another study suggested that resting-state FC fluctuations reflected both the continuous stream of ongoing cognitive process as well as the fixed anatomical connectivity matrix.[40]

The above studies showed that the dynamic FC could depict the underlying ongoing cognitive process during rest. Furthermore, the spatiotemporal dynamics of brain networks during task may provide more insights into the adaptation of the brain in response to modulated cognitive processes.[23,24] However, investigation on the task-related modulation of dynamic FC is still in an early stage. To the best of our knowledge, only one study has used dynamic FC to investigate the task-related modulation of FCV[41] so far, and found significant task-related decreases of FCV at the regional, network and system levels. In addition, the task-induced decrease in FCV was significantly correlated with task performance. It was proposed that the task-related reduction in FCV was likely related to the stabilization of the FC pattern to a certain task-specific functional organization. Nevertheless, FCV is still a relatively simple measure, which can only quantify the overall temporal pattern of dynamic FC, but ignore the spatial pattern of the networks. New methods are needed to depict the detailed spatiotemporal dynamics of brain networks during both rest and task. Thus, we propose to use k-means clustering to investigate spatiotemporal patterns of dynamic brain networks during both rest and task. Based on previous findings by static and dynamic FC analysis, we hypothesize the presence of overall spatial similarity but distinct temporal patterns between the rest and task.

In order to test this hypothesis, we analyzed the spatiotemporal patterns of the principal dynamic FC states at rest and how they were modulated spatiotemporally by a task. The hand closing-and-opening (HCO) task was utilized in this study for its easiness to perform and its ability to effectively activate the motor system,[42–44] and its extensive interests in studies on upper limb rehabilitation after stroke.[45–47] Investigating the alteration of the dynamic brain networks during HCO may also help understand the mechanisms underlying stroke rehabilitation. In addition to the motor-related networks (represented by MN hereafter) activated by HCO, DMN has also been demonstrated to be a key network in motor task performance and other cognitive processes.[1,48,49] Studying the dynamic relationships between MN and DMN during rest as well during HCO could help to reveal the brain's cognitive adaptation to task demands. Therefore, both DMN and MN were of interest in this study. Principal dynamic FC states were identified by k-means clustering of sliding windows.[22,36] We then compared the spatiotemporal patterns of principal FC states as well as the FCV under both rest and HCO conditions.

2. Materials and Methods

2.1. *Participants*

28 healthy right-handed subjects volunteered for this study and two subjects were excluded because of excessive head motions (maximal head motion above 2 mm or 2°). As a result, data of the 26 subjects (male/female: 13/13; age: 54.9 ± 6.3 years) were used for further analysis. All subjects provided the written informed consents. Procedures were reviewed

and approved by the Ethics Committee of Shanghai Second People's Hospital, Shanghai, China.

2.2. *Task design*

The fMRI experiment for each subject consisted of two FC sessions (REST and HCO) and one block-design activation session. During REST session, subjects were instructed to remain motionless, relaxed and awake. During HCO session, subjects were asked to perform HCO with the instructed hand at a rate of one time per second, paced by the cues on the display. In both REST and HCO sessions, 4 min and 20 s data were used for FC analysis. The third session was a block-design task consisting of six REST blocks alternated with five HCO task blocks, preceded by an 8 s inter-task period. Each block lasted for 20 s. This block-design session was used to generate candidate ROIs of the MN for FC analysis. All subjects were divided into the left-hand group (LHG, $n = 16$) or the right-hand group (RHG, $n = 10$). Subjects were instructed to use their hands as required during HCO task performance.

2.3. *Image acquisition*

All images were acquired with a 3.0 T Signa Excite Gemse MRI system (GE Healthcare, Milwaukee, WI, USA) at Rui Jin Hospital, School of Medicine, Shanghai Jiao Tong University, Shanghai, China. The head of the subject was snugly fixed by a foam pad to reduce head movements and scanner noises. Three-dimensional (3D) structural MRI was acquired from each subject using a T1-weighted MPRAGE sequence (TR = 5.6 ms; TE = 1.7 ms; flip angle = 12°; matrix size = 256 × 256; voxel size = 1 × 1 × 1 mm^3), yielding 196 contiguous sagittal slices (1 mm thick) covering the whole brain. Blood-Oxygenation-Level-Dependent (BOLD) data were acquired with an EPI sequence (TR = 2000 ms; TE = 30 ms; flip angle = 90°; matrix size = 64 × 64; voxel size = 3.75 × 3.75 × 4 mm^3) for each subject.

2.4. *FC data preprocessing*

For both REST and HCO periods, identical preprocessing procedures were performed using SPM8 (Wellcome Trust Centre for Neuroimaging, University College London, London, UK) and MATLAB scripts from the DPARSFA toolbox.[50] The data of the first 10 s (five volumes) were discarded to avoid magnetization equilibrium effects and to allow the subjects to get ready for the experiments. The remaining fMRI data were spatially realigned to the mean image and then were slice-timing corrected using the middle slice as the reference frame, detrended and band-pass filtered (0.01–0.08 Hz). In addition, the fMRI data were co-registered with each subject's anatomical data using mutual information as the cost function. fMRI data were interpolated using 4th degree B-spline method.[50] for its lower spatial resolution than anatomical images. The anatomical images were then segmented.[51] Spherical ROIs with 10 mm diameter were centered at predefined coordinates and warped to the subject's native brain-space based on the deformation field obtained from segmentation step. The representative BOLD time course for each ROI was defined as the average over all voxels within the ROI in the native brain space. Nuisance covariates, including Friston 24 parameters of head motion,[52] white matter and cerebrospinal fluid signals were then regressed out from the representative BOLD time courses.

2.5. *Motor network ROI identification*

In order to define the motor-related brain regions, activation based on block-design session was analyzed. Separate preprocessing was performed for block-design session data with SPM8 and DPARSFA toolbox, including spatial realignment to the mean volume of a series of images, slice-timing correction, co-registration, spatial normalization to the Montreal Neurological Institute (MNI) template, spatial smoothing (4 mm isotropic kernel) and high-pass filtering (eliminating slow signal drifts with a period longer than 128 s). For the first-level analysis of each subject, generalized linear model (GLM) in SPM8 was used to generate the individual activation map. Boxcar vectors for task blocks were convolved with the hemodynamic response function (HRF) and the head movement parameters were included as covariates to remove head motion artifacts. One-sample t-test based on single-subject contrasts obtained in the first-level analysis were performed for LHG and RHG, respectively, resulting in group-level activation mappings ($p < 0.001$) (see Table A.1 in Appendix A for details). By combining group-level activation maps of LHG and

RHG, we obtained the MNI coordinates of 44 activated motor-related brain regions (see Table A.2 in Appendix A for details).

2.6. *Analysis of dynamic FC*

ROIs in this study included regions in MN and DMN. For MN, the coordinates of the 44 activated local maxima obtained during the block-design session were regarded as the coordinates of ROIs. The coordinates of the 46 ROIs in DMN were defined according to Ref. 54 (Table A.3 in Appendix A for details). Thus, there were a total of 90 ROIs in the network-of-interest (denoted as DMN-MN hereafter) in total. The representative BOLD time courses of all ROIs were obtained by the methods in Data Preprocessing section.

For each subject, representative BOLD time courses of REST and HCO were analyzed by sliding windows (size: 30 TRs or 60 s each) with a step of 1 TR (2 s), resulting in 96 windows in total.[36,41] Within each sliding window, Fisher-transformed correlations were calculated between representative BOLD time courses of every pair of ROIs and a 90×90 association matrix was estimated.

2.7. *Clustering*

In order to identify reoccurring FC states, the k-means clustering algorithm[54] was implemented to classify the sliding windows into a set of separate clusters by their association matrices. $L1$ distance function (Manhattan distance or $L1$-norm) defined as

$$d_1(\mathbf{p}, \mathbf{q}) = \sum_{i=1}^{n} |(p_i - q_i)| \tag{1}$$

was used to estimate the within- and between-clusters distances,[55] where $d_1(\mathbf{p}, \mathbf{q})$ represents the $L1$ distance between two vectors $\mathbf{p}, \mathbf{q}$ in an n-dimensional real vector space, p_i and q_i represent the ith elements of $\mathbf{p}$ and $\mathbf{q}$, respectively.

As described by Allen and colleagues,[36] two-step clustering was used. In the first step, the sliding windows with local maxima in spatial variance of association matrices were selected as exemplars for each subject. Then, k-means clustering was performed on those exemplars selected from subjects. The clustering was repeated 100 times independently with a random initial centroid position every time and the best result was selected so as to increase the chance of escaping the local minima. The optimal number of clusters was determined based on the elbow criterion of cluster validity index, i.e. the ratio of within-cluster distances to between-cluster distances using k from 2 to 10.[36] For LHG, one set of exemplars was selected from sliding windows of 16 subjects for REST and HCO, respectively. For the clustering of exemplars in LHG, the optimal numbers of clusters were estimated as 6 (i.e. $k = 6$) in each session (REST and HCO). With respect to RHG, identical procedures were performed and $k = 4$ was estimated as optimal in each session (REST and HCO). In the second step, the centroids of resulting clusters for each session and each group were used to initialize the clustering used in the analysis of the full sliding time-windows.

2.8. *FCV analysis*

FCV was estimated to further examine the temporal patterns of dynamic FC during both REST and HCO in each network: DMN, MN, DMN-MN and the inter-network connecting DMN and MN (denoted as iDMN-MN hereafter). FCV of a network was estimated by calculating the standard deviation of the averaged FC strength in a network across all sliding time-windows,[39,41] that is,

$$\mathrm{FCV} = \sqrt{\frac{1}{M} \times \sum_{i=1}^{M} (\bar{x}_i - \bar{X})^2}, \tag{2}$$

where $\bar{x}_i$ represents the mean strength of FC among networks in the ith window, $\bar{X}$ represents the mean of $\bar{x_i}$ across all sliding windows, and M is the number of the windows.

2.9. *Statistical analysis*

In order to evaluate how the task modulated the temporal patterns of FC states, the frequency of state shifting (number of shifting times between FC states within 125 TR-long recording time) was compared between REST and HCO for both LHG and RHG. Since the frequency of state shifting was count data, they did not follow a normal distribution and ANOVA was not considered statistically appropriate.

According to previous studies, GLM with Poisson-distributed error can be used to perform statistical analysis for count data.[56,57] Nonetheless, the

Poisson distribution requires the mean equals to the variance, whereas the variance of our data was significantly larger than the mean, which is called "overdispersion". Thus, the best option for our data is to specify that the data follow the negative binomial distribution according to the previous studies.[58,59] A GLM with negative binomial-distributed error was used to examine the effect of session (REST versus HCO) as well as group (LHG versus RHG) on the state shifting frequency.[58,59] The negative binomial regression model is as follows:

$$\tilde{\mu}_{ij} = \exp(\alpha + \beta_1 s_j + \beta_2 g_i), \tag{3}$$

where $\tilde{\mu}_{ij}$ is the expected state shifting frequency for subject i ($i = 1$ to N; $N = 26$) during session j (REST and HCO), s_j represents the categorical variable of the session (i.e. $s_j = 1$ for REST; $s_j = 0$ for HCO), g_i represents the categorical variable of the group (i.e. $g_i = 1$ for subjects in LHG, $g_i = 0$ for subjects in RHG), β_1 and β_2 are the coefficients to be estimated and α is the intercept. If the estimated β_1 is significantly greater (less) than zero, the statistical result would indicate that the state shifting frequency during REST is greater (less) than that during HCO. If the estimated β_2 is significantly greater (less) than zero, the statistical result would indicate that the state shifting frequency of LHG is greater (less) than that of RHG. Incidence rate ratio (IRR, i.e. $\exp(\beta)$) was calculated,[59] which indicates the relative difference of state shifting frequencies between two categories (e.g. REST versus HCO; LHG versus RHG). Taking β_1 as an example, with all other factors being equal, the greater the IRR(β_1) is, the greater the state shifting frequency in REST is, compared with that in HCO. In addition, the Chi-square goodness-of-fit test was conducted to how much the data could fit a negative binomial model.[60]

3. Results

3.1. *FC states by k-means clustering*

As estimated by the elbow criterion of cluster validity, which was calculated as the ratio of within-cluster distance to between-cluster distance following the previous studies,[36,37] the optimal number of clustering FC states was six in LHG and four in RHG in both REST and HCO states. In both groups, only two principal FC states were identified in all subjects (see Fig. A.1 in Appendix A for details) during REST. The remaining FC states during REST (four FC states in LHG and two FC states in RHG) were absent in multiple subjects. While in HCO condition, only one principal FC state was identified in each group (see Fig. A.1 for details). Centroids of the principal FC states for REST and HCO in both groups were illustrated in Fig. 1. Similarities of principal FC states between LHG and RHG were estimated through correlational analysis, indicating significant similarities between the principal FC states in two groups (i.e. the first principal FC state of LHG REST and RHG REST: $R = 0.619$, $p < 0.001$; the second principal FC state of LHG REST and RHG REST: $R = 0.449$, $p < 0.001$; the first principal FC state of LHG HCO and RHG HCO: $R = 0.672$, $p < 0.001$). In addition, in both groups, significant similarity was observed between the principal FC state in HCO and the first principal FC state in REST (i.e. LHG: $R = 0.716$, $p < 0.001$; RHG: $R = 0.626$, $p < 0.001$).

3.2. *Dwell time ratios of principal FC states in REST*

To understand the temporal patterns of dynamic FC in REST, we examined the "dwell time" of the two principal FC states in REST. Dwell time ratio, i.e. the number of windows in one principal FC state over the total number of windows, was defined to quantify the "dwell time" of the corresponding state. Mixed-design ANOVA with one between-subjects variable (i.e. GROUP: LHG versus RHG) and one within-subjects variable (i.e. STATE: the first principal FC state versus the second principal FC state) was performed. The main effect of STATE was significant ($F(1, 19) = 4.773$, $p = 0.042$), but the main effect of GROUP was not observed (Fig. 2). The statistical results demonstrated that the "dwell time" of the first principal FC state was significantly longer than that of the second principal FC state in REST for either LHG or RHG.

3.3. *Difference between two principal FC states in REST*

In addition to "dwell time", FC pattern between the two principal FC states was also investigated for both LHG and RHG. Paired t-test showed significantly different FC between two principal FC states in REST ($p < 0.01$). For LHG (Fig. 3(a)), among the

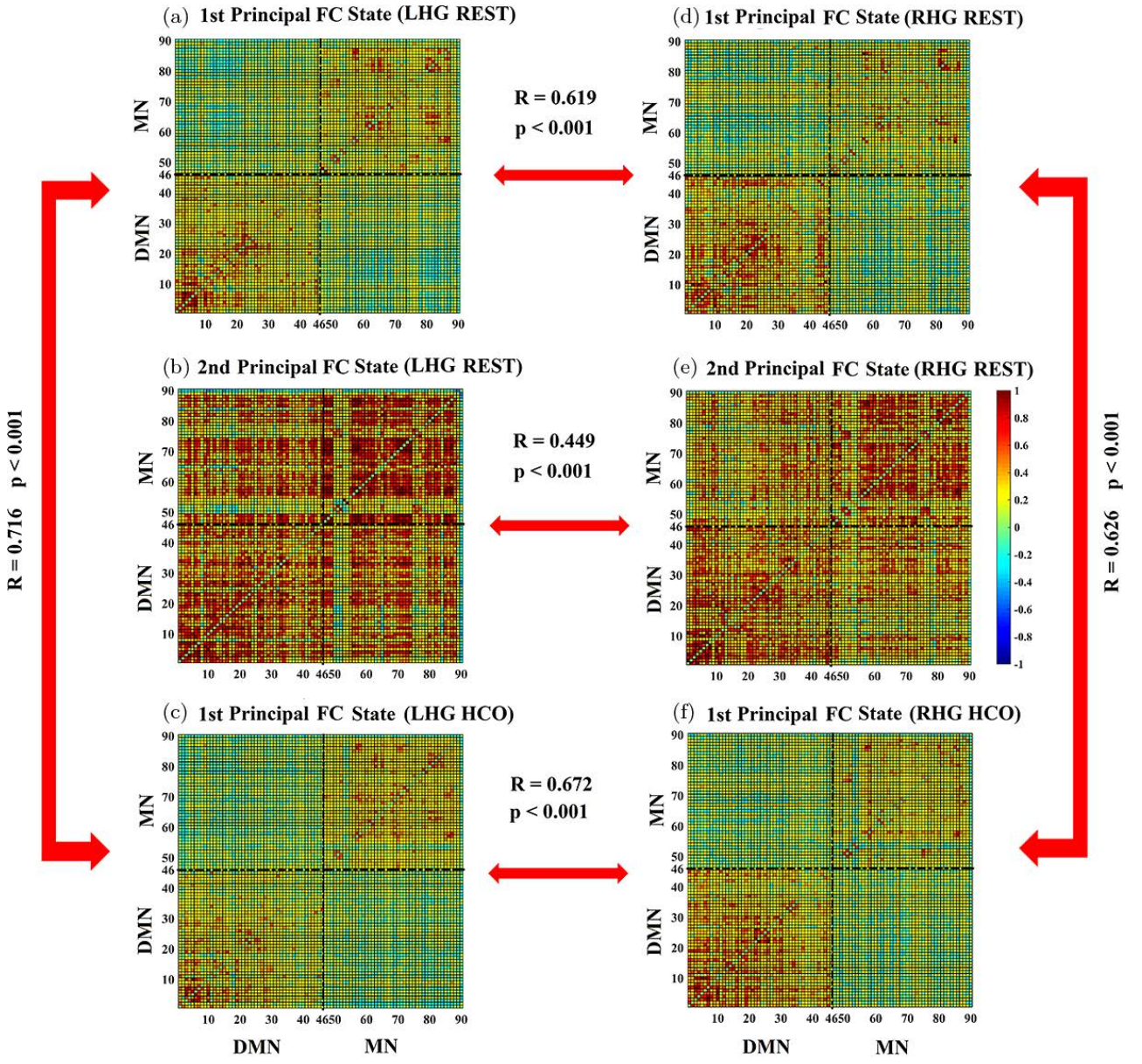

Fig. 1. (a, b) Centroids of two principal FC states of REST in LHG; (c) centroid of the only principal FC state of HCO in LHG; (d, e) centroids of two FC principal FC states of REST in RHG and (f) centroid of the only principal FC state of HCO in RHG. DMN: ROI 1 to ROI 46; MN: ROI 47 to ROI 90.

132 significantly different connections, 13 (percentage in all connections in DMN: 13/1035 = 1.26%) corresponded with the DMN, and 46 (46/946 = 4.86%) were found in the MN and 73 (73/2024 = 3.61%) were present in the iDMN-MN. For RHG (Fig. 3(e)), 147 significantly different connections were identified, with 11 (1.06%) located in the DMN, 41 (4.33%) in the MN, and 95 (4.69%) were associated with iDMN-MN. For both LHG and RHG, all significantly different connections increased in strength during the second principal FC state in contrast to the first principal FC state of REST. The majority of significantly different connections were located in the iDMN-MN for both LHG and RHG. As the matrix of principal FC state was symmetric, only the lower part of diagonal was shown in Figs. 3(a) and 3(c). Figure 3 also presents the ROIs and significant connections between other regions.

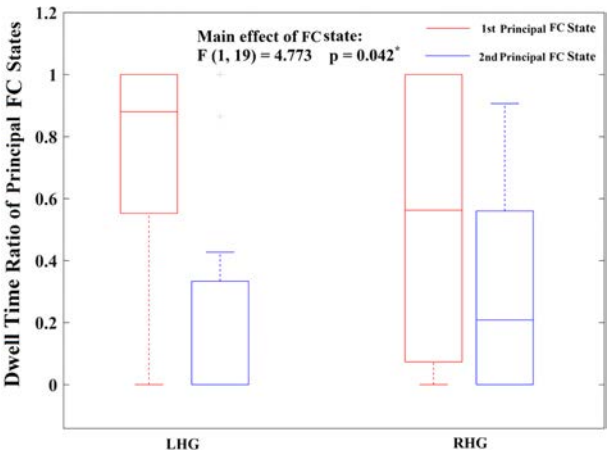

Fig. 2. Boxplots of dwell time ratio of principal FC states in LHG and RHG in REST.

We observed that there were less significantly different connections in the DMN compared with MN and iDMN-MN networks in both LHG and RHG groups.

In addition to the specific differences in FC, the overall similarities of the DMN, MN, and iDMN-MN networks with the principal FC states were also investigated by correlational analysis (correlation coefficient was r-to-z transformed by Fisher transformation) for each subject. Mixed-design ANOVA with one between-subjects variable (i.e. GROUP: LHG versus RHG) and one within-subject variable (i.e. NETWORK: DMN, MN, and iDMN-MN) was performed. Post-hoc comparisons of transformed correlation coefficients in each network (i.e. DMN, MN and iDMN-MN) were adjusted using Bonferroni correction. It was noted that the transformed correlation coefficients of iDMN-MN between the principal FC states were significantly smaller than those of either DMN or MN (Fig. 4).

3.4. *Differences in state shifting frequency between REST and HCO*

In order to compare the dynamic patterns of the networks in REST and HCO, we investigated the state shifting frequency (i.e. number of shifting times across different FC states including nonprincipal states) in both groups. Table 1 lists the results of negative binomial regression model estimation. The estimated coefficient for session type variable (1 for REST and 0 for HCO) was positive and significantly different than zero ($p = 0.030$). Even though the coefficient of group variable (1 for LHG and 0 for RHG) was also positive, it did not significantly differ from 0. The IRR for the session variable was 3.212, indicating that with all other factors being equal, an average increase of 212.2% in the state shifting frequency was observed during REST compared with HCO. The statistical results suggest that state shifting frequency was significantly increased during REST compared with HCO in either group. In addition, Chi-square goodness-of-fit test suggested that the negative binomial model could be appropriately used to fit the data since the null hypothesis that the data were consistent with the negative binomial model could not be rejected ($p = 0.191$).

3.5. *Different FCV between REST and HCO*

For each subject, the FCVs of DMN, MN, DMN-MN, iDMN-MN were calculated for both REST and HCO. Mixed-design ANOVA with one between-subject variable (i.e. GROUP: LHG versus RHG) and one within-subject variable (i.e. SESSION: REST versus HCO) was performed for each network examining the effect of session on the FCV. Significant main effect of session type was found on FCV of the DMN-MN ($F(1, 24) = 5.466$, $p = 0.028$), MN FC ($F(1, 24) = 9.131$, $p = 0.006$) and iDMN-MN FC ($F(1, 24 = 6.404$, $p = 0.018$) (Fig. 5). These results suggest that the FCV of the DMN-MN network, MN, and iDMN-MN significantly decreased during HCO compared with REST for both LHG and RHG groups.

4. Discussion

In this study, the dynamic FC of brain networks including DMN and MN, as well as their variability (FCV), was examined using sliding windows and k-means clustering. Principal FC states were identified and their spatiotemporal patterns were compared between REST and HCO. During REST, two principal FC states were identified in both the LHG (Figs. 1(a) and 1(b)) and RHG (Figs. 1(d) and 1(e)), with significant similarities between the two groups. For HCO, a single principal FC state was identified in LHG (Fig. 1(c)) and RHG (Fig. 1(f)), which also featured a significant similarity between the two groups. These results indicated a correspondence of principal FC states between two groups in both REST and HCO experimental conditions. When comparing

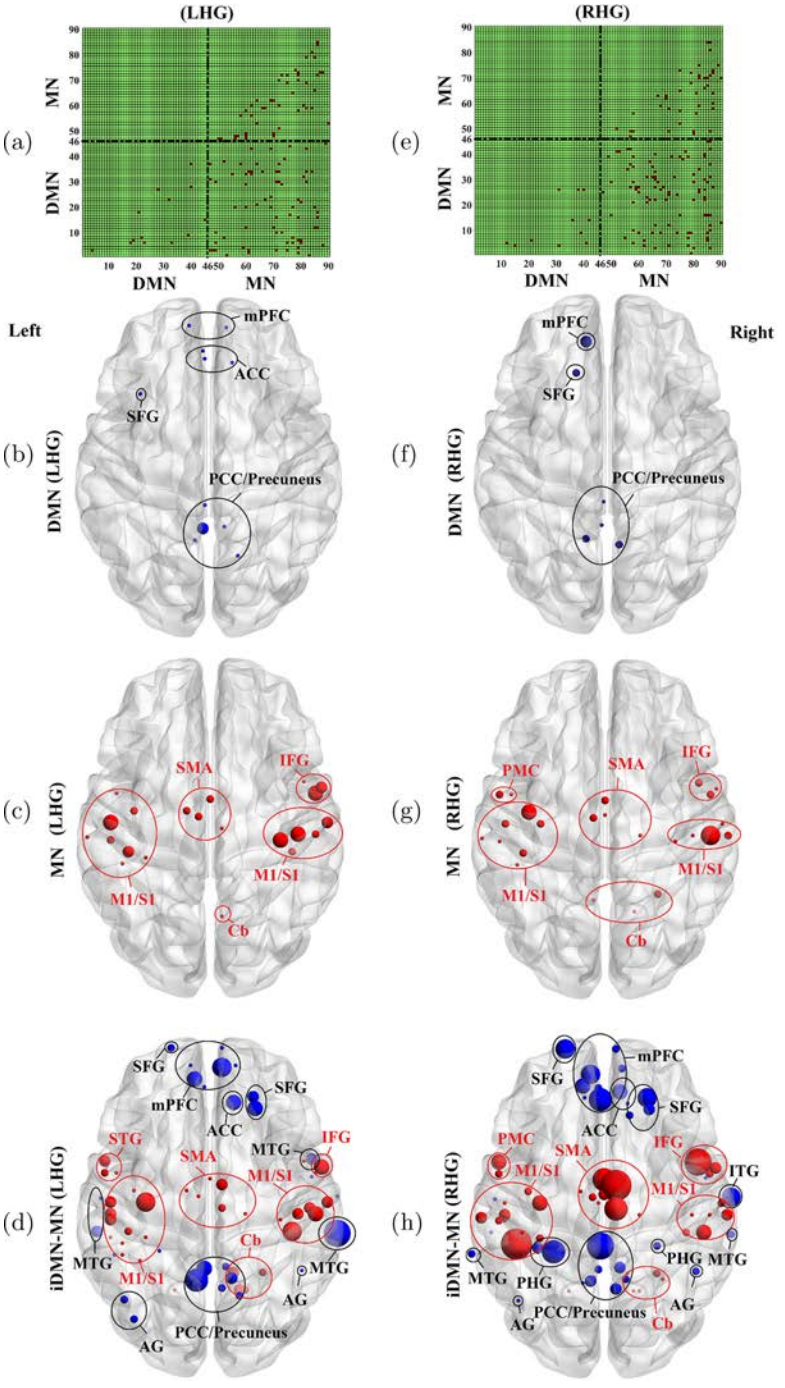

Fig. 3. (Color online) Illustration of significantly different FC between the principal FC states of REST in LHG (a) and RHG (e); ROIs in DMN (blue nodes) connected by significantly different DMN FC in LHG (b) and RHG (f); ROIs in MN (red nodes) connected by significantly different MN FC in LHG (c) and RHG (g); and ROIs in DMN (blue nodes) and MN (red nodes) connected by significantly different iDMN-MN FC in LHG (d) and RHG (h). The size of the nodes indicates the ROI degree of connectivity (i.e. the number of significantly different FC connected to ROI). *Notes:* PCC = posterior cingulate cortex; mPFC = medial prefrontal cortex; SFG = superior frontal gyrus; MTG = middle temporal gyrus; M1 = primary motor cortex; S1 = primary somatosensory cortex; SMA = supplementary motor cortex; STG = superior temporal gyrus; ACC = anterior cingulate cortex; IFG = inferior frontal gyrus; PMC = premotor cortex; AG = angular gyrus; Cb = cerebellum; PHG = parahippocampal gyrus.

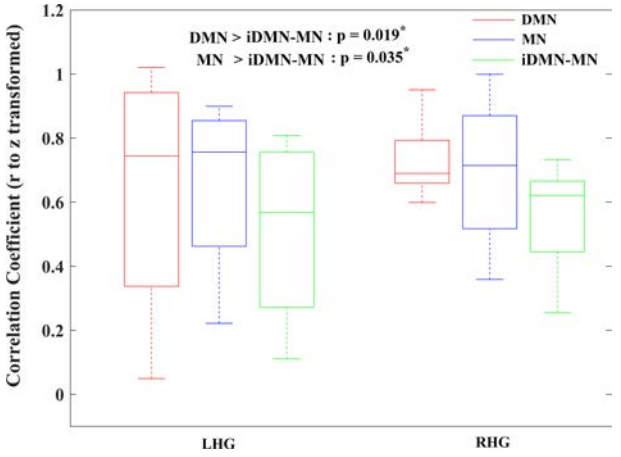

Fig. 4. Boxplots of similarities (indicated by correlation coefficient, which was r to z transformed) of DMN, MN, and iDMN-MN between two principal FC states in REST for LHG and RHG, respectively.

Table 1. Estimated coefficients of negative binomial regression model for IRR in state shifting frequency.

	Estimate (IRR)	Std. error	Z-value	P-value
(Intercept)	−1.486	0.582	−2.554	0.011*
Coefficient (Group)	0.673 (1.960)	0.558	1.206	0.228
Coefficient (Session)	1.167 (3.212)	0.537	2.171	0.030*

*indicates the estimate is significant different from zero.

principal FC states in REST and HCO, significant similarity was also found between the single principal FC state in HCO and the first principal FC state in REST regardless of the hand used (Fig. 1). This finding verified our hypothesis on the overall spatial similarity of dynamic FC between rest and task states.

Previous studies on static FC have observed overall FC similarity between rest and task.[14–16] Specifically, Cole and colleagues used static FC to investigate the similarities of large-scale networks, which covered hundreds of brain regions encompassing every major brain system between dozens of task sessions and the resting state. Their results proposed that task-state functional networks were shaped primarily by an intrinsic network architecture that was also presented during rest, and secondarily by evoked task-related network changes.[17] In another study on the relationship between structural connectivity (SC) and FC, Hermundstad and colleagues found that structural properties (i.e. length, number and spatial location of white matter fibers) were indicative of the strength of FC in both rest and task states.[61] These results based on static FC both proposed that the brain networks during both rest and task states might be primarily shaped by a common intrinsic network architecture. Our dynamic FC study found similar principal FC states between REST and HCO, which were the first principal FC state in REST and the only principal FC state during HCO. We observed that these two related principal FC states were dominant during REST and HCO as measured by dwell time ratios (Fig. 2). Thus, we speculate that the common intrinsic network architecture, which primarily shapes both resting-state and task-state network in static FC study, presents itself in similar dominating principal FC states observed in REST and HCO. Despite these similarities with static analysis, dynamic FC can provide more information than static FC. The second principal FC state in REST might reflect a specific mental activity in REST not presented during HCO, and its absence in HCO might represent a focus on motor task execution. A previous study demonstrated that mental activity during rest was unconstrained and individuals could freely engage in several types of mental activity.[62] This unconstrained mental activity might be represented in part by the second principal FC state of REST in this study.

Though the second principal FC state in REST might indicate unconstrained mental activity during REST, what kind of brain activity it represents and its role in the "default mode", especially for motor system, are still not well understood. From the perspective of individual connection changes in FC, differences between two principal FC states in REST were most numerous in the iDMN-MN and MN. In addition, all significantly different functional connections increased in strength during the second principal FC state compared with the first principal FC state (Fig. 3). Furthermore, from the perspective of overall network pattern, the differences between these two principal FC states were mainly observed in the iDMN-MN (Fig. 4). Strengthened correlation between DMN and MN during the second principal FC state of REST, is consistent with previous findings that core ROIs in DMN, such as PCC, most frequently engaged with non-DMN ROIs

through inter-network FC.[39,63] A recent study using network control theory investigated how the brain shifts between cognitive states based on network organization of white matter microstructure. The authors found that the "default mode" during resting state was a pluripotent "ground status" which was easily able to migrate to multiple task-based statuses with less cognitive effort by using connections between DMN and other networks.[64] Taken together with these findings, our results imply that during the REST, DMN could be coordinating with MN, manifested by the second principal FC state, to establish a "default mode" of the MN and prepare for the subsequent motor tasks. During HCO itself, maintaining the "default mode" in motor system may have been not necessary, resulting in an absence of a second principal FC state.

In addition, according to the model described in Table 1, the maintenance of "default mode" for motor system in REST might be a dynamic process, that is, the dynamic FC in DMN-MN network could be observed to frequently shift between the two principal FC states. Concordantly, FCV of the DMN-MN network significantly decreased during HCO compared with REST (Fig. 5(a)), a finding which was also in line with recent findings during an attention task.[41] With respect to the individual networks, FCV of MN and iDMN-MN also decreased during HCO (Figs. 5(c) and 5(d)), while no significant change of FCV was observed in DMN (Fig. 5(b)). Considering the findings of principal FC states, the increase of FCV in iDMN-MN and MN was probably due to the frequent shift between the principal FC states in REST as the differences between two principal FC states were mainly located in iDMN-MN and MN. During HCO, such a dynamic maintenance of "default mode" in motor system would disappear and result in a stable and lower FCV in iDMN-MN and MN,[65] indicating more temporally stable dynamic brain networks during HCO. These findings verified our hypothesis that differences in temporal patterns of dynamic FC between REST and HCO still existed and could reflect distinct mental states present in REST and HCO.

Unlike the MN and iDMN-MN, the FCV of DMN did not change significantly in HCO compared with REST, implying a special role for the DMN in REST and HCO. During the REST, the DMN might not only interact with MN, but also with other networks such as the auditory network, attention network, etc. When involved in a motor task, the MN and iDMN-MN were relatively stable due to an absence of influence of DMN on the motor system, but the DMN might still be coordinating with other networks to establish a "default-mode" for other brain functions. Previous studies reported that the FCV during resting state was partially caused by the predominance of mind-wandering or day-dreaming during this "uncontrolled" state.[39,41] Another study suggested that mind-wandering might be part of a larger class of mental phenomena that

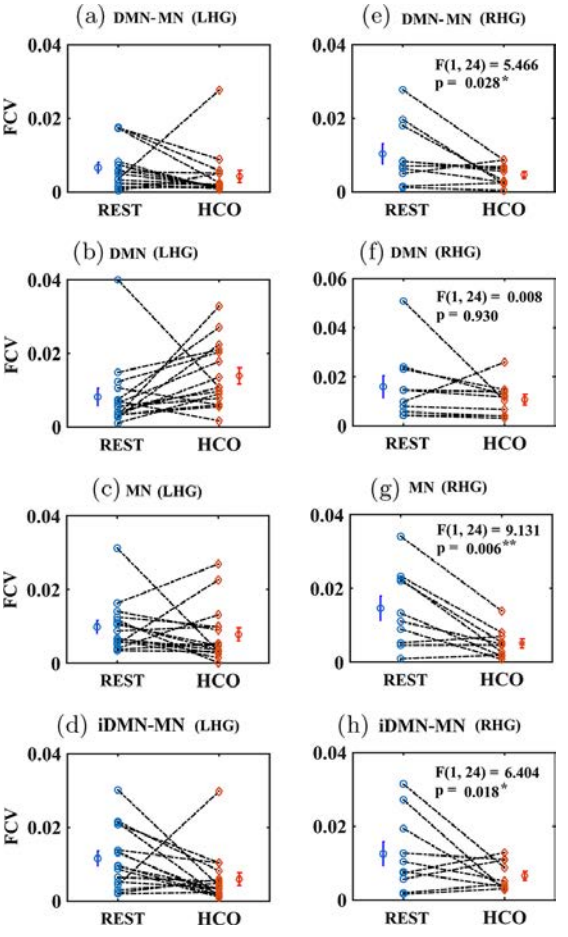

Fig. 5. (Color online) Demonstration of FCV in the DMN-MN during REST and HCO in the LHG (a) and RHG (e); FCV in the DMN in LHG (b) and RHG (f); FCV in the MN in LHG (c) and RHG (g); and FCV in the iDMN-MN in LHG (d) and RHG (h). Blue circles and each red diamonds represent FCV during REST and HCO, respectively, for individual subjects. Error bars with corresponding markers represent the mean and its standard error of mean (SEM) across subjects.

enable executive processes without diminishing the potential contribution of DMN to other cognitive functions.[66] These descriptions correspond to our speculation that DMN was coordinating with multiple function-related networks during REST and its coordinating with nonmotor networks was not diminished during HCO.

In general, previous studies have used dynamic FC to investigate either the dynamic brain networks during rest[36,39,40,67,68] or how the resting-state FCs are related to the physiologic or pathologic states.[37,38] However, in this study, we aim to investigate how the motor task would affect the brain networks spatiotemporally, and particularly, how brain networks establish the "default mode" and reorganize spatiotemporally in response to a task. By k-means clustering, this study found overall spatial similarity of primary principal FC states, but distinct temporal patterns of principal FC states between rest and task states. Our findings could explain the consistent network configuration,[17] but distinct FCV[41] between rest and task states. In addition, previous study only examined the FCV during task,[41] while this study adopted k-means clustering, to reveal the spatiotemporal details in the brain networks during both rest and task states.

Furthermore, we would like to discuss several methodological issues. First, Lloyds algorithm of k-means clustering was used in this study.[54] The computation complexity of the algorithm is $O(nkdi)$, where n is the number of d-dimensional vectors, k is the number of clusters and i is the number of iterations for convergence. Taking the HCO data of LHG as an example, the total computation time was 377.11 s.

Second, we note that the correlation between a pair of BOLD time series is not an adequate indication of a direct communication between two brain regions, and it could be driven by a common source elsewhere, though the neural correlates of FC[69–71] and the correlation between FC and structural connections[72,73] have been reported. However, in this study, we only interpreted the increase of FCs between DMN and MN in the second principal FC state as a strengthened functional relationship between the two networks, no matter the functional relationship is direct or not. In spite of such a limitation, FC is still one of the best measures to depict the correlation between brain regions in non-invasive neuroimaging studies and has been widely applied to cognitive neuroscience, neurological and psychiatric disorders.[74–78]

Third, with respect to the interpretation of FC fluctuation, a recent study suggested that the correlation fluctuations could still exist between regions with distinct amplitude spectra, whether or not there are dynamic changes in neural connectivity between them. That study also suggested that multivariate analysis could distinguish the FC fluctuations caused by neural activities.[79] In this study, we used k-means clustering, which is a multivariate analysis method, to spatiotemporally cluster the FCs over all sliding windows, connections and subjects into principal states. Thus, the fluctuations of the principal states were not likely determined by the sliding window correlation method only. Furthermore, we created surrogate data by phase randomization in Fourier domain, which preserved the mean, variance, amplitude spectra and temporal autocorrelation, but disturbed the covariance structure of original BOLD time series.[80,81] The results showed that the surrogate data had distinct spatiotemporal patterns compared with original BOLD time series (see Figs. A.2(a) and A.2(b) in Appendix A for details) and the principal FC state of surrogate data did not show any meaningful FC patterns like those in the original BOLD time series (see Figs. A.2(c) and A.2(d) in Appendix A for details), which further supported that our findings of the FC spatiotemporal patterns were not inherent from the method, but with biological significance. In addition, several previous studies have also demonstrated the biological significance of FC fluctuations.[39–41]

Finally, several limitations in this study should be noted. First, the fMRI scan time period was relatively short. Longer scanning time would increase the reliability of the estimation of FC dynamics. Second, FC states were identified by k-means clustering, which although known as an efficient and robust method with a tendency to converge at a local minima. So, in this study, the clustering algorithm was repeated 100 times independently with random initial centroid position every time to increase the chance to escape the local minima.

In addition, there are alternative clustering methods (e.g. density-based or fuzzy-clustering method), which may be better suited to dynamic FC analysis and worthy of further investigation in further work. Third, our study only investigated FC reorganization with a motor task. Further studies on tasks involving other cognitive domains should be done to examine whether similar findings would exist for other cognitive processes.

5. Conclusions

This study examined FC states and FCV in REST and HCO using sliding windows and k-means clustering. Two principal FC states in REST and one principal FC state in HCO were identified. The first principal FC state in REST was similar to that in HCO, which likely represented intrinsic network architecture and validated the broadly similar spatial patterns between REST and HCO. However, the presence of a second principal FC state with increased iDMN-MN in REST with shorter "dwell time" could imply the transient functional relationship between DMN and MN to establish the "default mode" for motor system. In addition, the more frequent shifting between two principal FC states in REST indicated that the brain networks dynamically maintained the "default mode" for the motor system. In contrast, during HCO, the presence of a single principal FC state and reduced FCV implied a more temporally stable connectivity, validating the distinct temporal patterns between REST and HCO. Our findings suggested that the principal states could show a link between the rest and task states, and verified our hypothesis on overall spatial similarity but distinct temporal patterns of dynamic brain networks between rest and task states. These results showed the effectiveness of dynamic FC analysis when applied to brain activities during rest and task states, and offer new insights into understanding the adaptation of brain networks in response to task performance.

Acknowledgments

This work was supported by National Key R&D Program of China (No. 2017YFC0909201), the National Natural Science Foundation of China (Nos. 61571295 and 61673267), funding for "outstanding principal investigator of Health Systems" in Huangpu District, Shanghai, and Natural Science Foundation of Shanghai (16ZR1446600).

Appendix A. Supplementary Materials

A.1. *Surrogate test*

To test the effectiveness of the k-means clustering method, we used a surrogate test to check differences in FC states between original data and surrogate

Table A.1. Activated ROIs of LHG and RHG.

			MNI coordinates (local maxima)		
T	Z	P-value	X (mm)	Y (mm)	Z (mm)
		LHG			
16.665	6.086	5.8×10^{-10}	45	−21	60
11.807	5.425	2.9×10^{-8}	36	−24	66
8.906	4.850	6.2×10^{-7}	54	−21	45
14.153	5.778	3.8×10^{-9}	−6	−54	−21
8.624	4.783	8.6×10^{-7}	6	−63	−21
8.167	4.668	1.5×10^{-6}	15	−60	−24
7.170	4.390	5.66×10^{-6}	−12	−9	27
5.385	3.769	8.2×10^{-5}	−12	0	27
6.774	4.268	9.87×10^{-6}	−18	−60	−57
5.917	3.974	3.53×10^{-5}	−6	−12	72
5.859	3.953	3.86×10^{-5}	0	−9	57
5.427	3.786	7.66×10^{-5}	0	−3	51
5.699	3.892	4.97×10^{-5}	54	0	21
4.125	3.193	0.000704	57	3	30
5.532	3.827	6.47×10^{-5}	51	−18	18
5.414	3.781	7.82×10^{-5}	60	−15	18
4.724	3.484	0.000247	63	−21	12
5.379	3.766	8.28×10^{-5}	−54	0	42
5.214	3.698	0.000108	−63	−21	15
5.186	3.687	0.000113	−45	−36	21
5.103	3.652	0.00013	18	−21	3
4.938	3.580	0.000172	−54	−24	24
4.895	3.561	0.000184	−51	−24	33
4.909	3.567	0.00018	−39	−9	60
4.462	3.361	0.000388	−33	−15	57
		RHG			
10.175	4.664	1.55×10^{-6}	−51	−15	42
10.086	4.649	1.67×10^{-6}	−42	−30	48

Table A.1. (*Continued*)

			MNI coordinates (local maxima)		
T	Z	P-value	X (mm)	Y (mm)	Z (mm)
7.473	4.119	1.89×10^{-5}	−33	−33	39
8.683	4.388	5.72×10^{-6}	27	−51	−27
7.964	4.234	1.15×10^{-5}	18	−60	−33
7.367	4.093	2.13×10^{-5}	12	−51	−27
8.119	4.269	9.84×10^{-6}	51	−30	30
5.496	3.551	0.00019	42	−30	33
7.921	4.224	1.19×10^{-5}	−54	6	0
6.977	3.994	3.24×10^{-5}	−48	0	0
7.411	4.104	2.03×10^{-5}	−51	−21	12
6.766	3.938	4.11×10^{-5}	−63	−24	12
5.961	3.704	0.00011	−51	−33	12
6.727	3.927	4.29×10^{-5}	48	6	3
6.583	3.888	5.06×10^{-5}	6	−18	66
5.707	3.623	0.00015	6	−6	57
5.526	3.562	0.00018	0	−12	57
5.435	3.531	0.00021	−3	−15	48
5.706	3.622	0.00015	−45	−42	27
4.506	3.179	0.00074	−36	−45	30
5.057	3.396	0.00034	30	−54	9

data. Surrogate data were created by phase randomization in Fourier domain.[80,81] As a result, the mean, variance and temporal autocorrelation of surrogate data generated from BOLD time series were identical to the original BOLD time series, but the covariance structure of each pair of original BOLD time series was disturbed by randomization.

Table A.2. MNI coordinates of 44 activated motor-related ROIs (two ROIs in LHG overlapped with two ROIs in RHG and were combined into two ROIs through spatially averaging).

No.	X (mm)	Y (mm)	Z (mm)	No.	X (mm)	Y (mm)	Z (mm)
1	45	−21	60	23	−51	−24	33
2	36	−24	66	24	−39	−9	60
3	54	−21	45	25	−33	−15	57
4	−6	−54	−21	26	−51	−15	42
5	6	−63	−21	27	−42	−30	48
6	15	−60	−24	28	−33	−33	39
7	−12	−9	27	29	27	−51	−27
8	−12	0	27	30	18	−60	−33
9	−18	−60	−57	31	12	−51	−27
10	−6	−12	72	32	51	−30	30

Table A.2. (*Continued*)

No.	X (mm)	Y (mm)	Z (mm)	No.	X (mm)	Y (mm)	Z (mm)
11	0	(−10.5)	57	33	42	−30	33
12	0	−3	51	34	−54	6	0
13	54	0	21	35	−48	0	0
14	57	3	30	36	−51	−21	12
15	51	−18	18	37	−51	−33	12
16	60	−15	18	38	48	6	3
17	63	−21	12	39	6	−18	66
18	−54	0	42	40	6	−6	57
19	−63	(−22.5)	13.5	41	−3	−15	48
20	−45	−36	21	42	−45	−42	27
21	18	−21	3	43	−36	−45	30
22	−54	−24	24	44	30	−54	9

In order to compare the spatiotemporal FC patterns between original data and surrogate data, FC similarity matrices for both original and surrogate data were generated, respectively. The (t_1, t_2) entry of the FC similarity matrix provided the Pearson correlation between the upper triangular parts of two FC matrices at t_1 and t_2. According to Figs. A.2(a)

Table A.3. MNI coordinates of 46 ROIs in DMN.[53]

No.	X (mm)	Y (mm)	Z (mm)	No.	X (mm)	Y (mm)	Z (mm)
1	−44	−65	35	24	−3	44	−9
2	−39	−75	44	25	8	42	−5
3	−7	−55	27	26	−11	45	8
4	6	−59	35	27	−2	38	36
5	−11	−56	16	28	−3	42	16
6	−3	−49	13	29	−20	64	19
7	8	−48	31	30	−8	48	23
8	15	−63	26	31	65	−12	−19
9	−2	−37	44	32	−56	−13	−10
10	11	−54	17	33	−58	−30	−4
11	52	−59	36	34	65	−31	−9
12	23	33	48	35	−68	−41	−5
13	−10	39	52	36	13	30	59
14	−16	29	53	37	12	36	20
15	−35	20	51	38	52	−2	−16
16	22	39	39	39	−26	−40	−8
17	13	55	38	40	27	−37	−13
18	−10	55	39	41	−34	−38	−16
19	−20	45	39	42	28	−77	−32
20	6	54	16	43	52	7	−30
21	6	64	22	44	−53	3	−27
22	−7	51	−1	45	47	−50	29
23	9	54	3	46	−49	−42	1

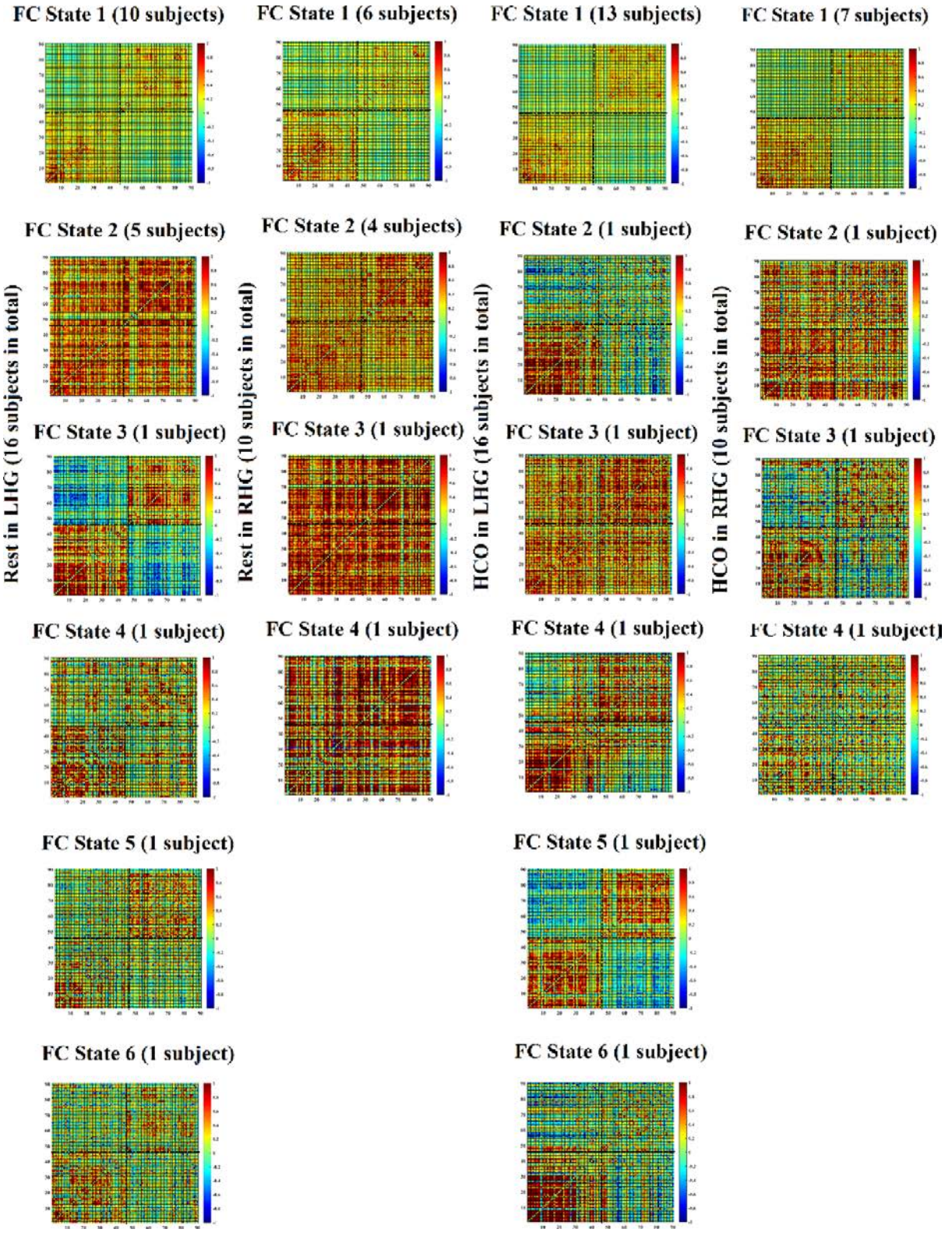

Fig. A.1. The FC states during Rest and HCO obtained through k-means clustering of sliding time-windows in LHG and RHG. The number of subjects for each FC state is also shown in the title. Principal FC states were identified as those that occurred in multiple subjects, while other observed FC states occurred in only a single subject.

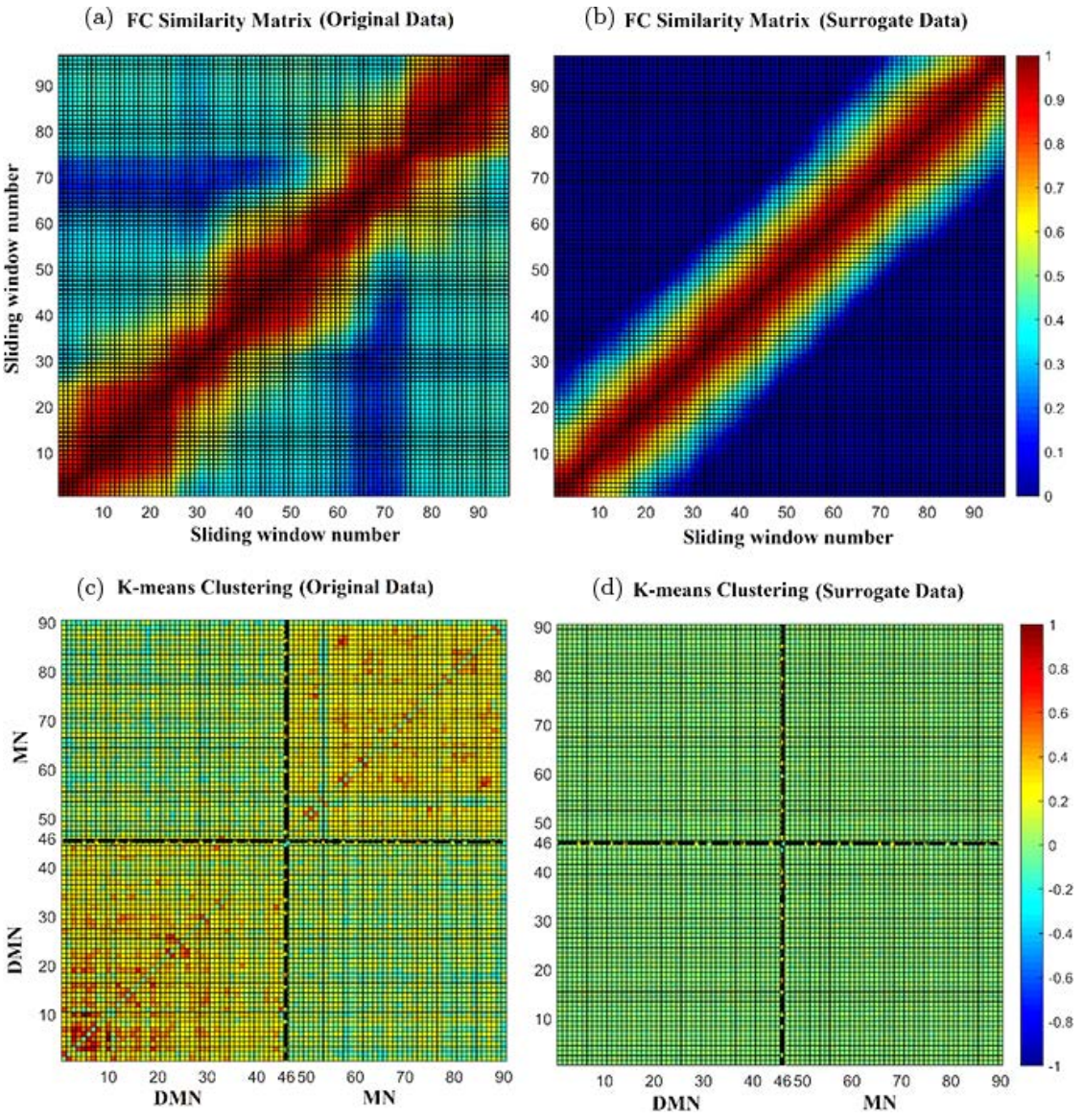

Fig. A.2. Illustration of the FC similarity matrices in original data (a) and surrogate data (b) of HCO in LHG as well as the centroids of principal FC states in original data (c) and surrogate data (d) for a typical subject.

and A.2(b), the spatiotemporal FC patterns of surrogate data were different from the original data. There were segments of sliding windows with similar FC patterns illustrated by blocks with high correlation coefficients along the diagonal in FC similarity matrices. For surrogate data, the sizes of these blocks were approximately constant across time, resulting in a strip with high correlation coefficients along the diagonal in the FC similarity matrix (Fig. A.2(b)), which was due to the inherent features of estimating dynamic FC through sliding windows as the adjacent windows had similar FC patterns. However, for the original data, the sizes of blocks varied across time (Fig. A.2(a)), which might be related to the underlying mental state.

If the clusters were inherent from the method rather than based on spatiotemporal FC patterns, the resulting clusters for surrogate data should resemble the original data. However, the principal FC states of surrogate data did not show any meaningful FC pattern like those observed in the original data. For example, the centroid of one principal FC state obtained from surrogated data of HCO for LHG (Fig. A.2(c)) does not show any network structures,

such as DMN and MN in original data (Fig. A.2(d)). Thus, these results demonstrated that the clusters were classified based on the spatiotemporal patterns of FCs.

References

1. D. A. Gusnard and M. E. Raichle, Searching for a baseline: Functional imaging and the resting human brain, *Natl. Rev. Neurosci.* **2**(10) (2001) 685–694.
2. M. E. Raichle *et al.*, A default mode of brain function, *Proc. Natl. Acad. Sci.* **98**(2) (2001) 676–682.
3. M. E. Raichle and D. A. Gusnard, Intrinsic brain activity sets the stage for expression of motivated behavior, *J. Comp. Neurol.* **493**(1) (2005) 167–176.
4. D. Mantini and W. Vanduffel, Emerging roles of the brain's default network, *Neuroscientist* **19**(1) (2013) 76–87.
5. J. R. Andrews-Hanna, The brain's default network and its adaptive role in internal mentation, *Neuroscientist* **18**(3) (2012) 251–270.
6. R. Yuvaraj *et al.*, Brain functional connectivity patterns for emotional state classification in Parkinson's disease patients without dementia, *Behav. Brain Res.* **298** (2016) 248–260.
7. Y. Yang *et al.*, A general approach for quantifying nonlinear connectivity in the nervous system based on phase coupling, *Int. J. Neural Syst.* **26**(1) (2016) 1550031.
8. M. Ahmadlou and H. Adeli, Complexity of weighted graph: A new technique to investigate structural complexity of brain activities with applications to aging and autism, *Neurosci. Lett.* **650** (2017) 103–108.
9. G. Mirzaei and H. Adeli, Resting state functional magnetic resonance imaging processing techniques in stroke studies, *Rev. Neurosci.* **27**(8) (2016) 871.
10. U. Hasson, H. C. Nusbaum and S. L. Small, Task-dependent organization of brain regions active during rest, *Proc. Natl. Acad. Sci.* **106**(26) (2009) 10841–10846.
11. B. J. Harrison *et al.*, Consistency and functional specialization in the default mode brain network, *Proc. Natl. Acad. Sci.* **105**(28) (2008) 9781–9786.
12. W. Gao and W. Lin, Frontal parietal control network regulates the anti-correlated default and dorsal attention networks, *Hum. Brain Mapp.* **33**(1) (2012) 192–202.
13. A. Fornito *et al.*, Competitive and cooperative dynamics of large-scale brain functional networks supporting recollection, *Proc. Natl. Acad. Sci.* **109**(31) (2012) 12788–12793.
14. D. A. Fair *et al.*, A method for using blocked and event-related fMRI data to study "resting state" functional connectivity, *Neuroimage* **35**(1) (2007) 396–405.
15. M. D. Fox *et al.*, Intrinsic fluctuations within cortical systems account for intertrial variability in human behavior, *Neuron* **56**(1) (2007) 171–184.
16. M. D. Greicius *et al.*, Functional connectivity in the resting brain: A network analysis of the default mode hypothesis, *Proc. Natl. Acad. Sci.* **100**(1) (2003) 253–258.
17. M. W. Cole *et al.*, Intrinsic and task-evoked network architectures of the human brain, *Neuron* **83**(1) (2014) 238–251.
18. M. Ahmadlou *et al.*, Complexity of functional connectivity networks in mild cognitive impairment subjects during a working memory task, *Clin. Neurophysiol.* **125**(4) (2014) 694–702.
19. A. Arieli *et al.*, Dynamics of ongoing activity: Explanation of the large variability in evoked cortical responses, *Science* **273**(5283) (1996) 1868–1871.
20. J. Onton *et al.*, Imaging human EEG dynamics using independent component analysis, *Neurosci. Biobehav. Rev.* **30**(6) (2006) 808–822.
21. C. Chang and G. H. Glover, Time–frequency dynamics of resting-state brain connectivity measured with fMRI, *Neuroimage* **50**(1) (2010) 81–98.
22. Ü. Sakoğlu *et al.*, A method for evaluating dynamic functional network connectivity and task-modulation: Application to schizophrenia, *Magn. Reson. Mater. Phys. Biol. Med.* **23**(5–6) (2010) 351–366.
23. R. M. Hutchison *et al.*, Dynamic functional connectivity: Promise, issues, and interpretations, *Neuroimage* **80** (2013) 360–378.
24. V. D. Calhoun *et al.*, The chronnectome: Time-varying connectivity networks as the next frontier in fMRI data discovery, *Neuron* **84**(2) (2014) 262–274.
25. M. Ahmadlou, H. Adeli and A. Adeli, Graph theoretical analysis of organization of functional brain networks in ADHD, *Clin. EEG Neurosci.* **43**(1) (2012) 5–13.
26. T. Koenig *et al.*, Millisecond by millisecond, year by year: Normative EEG microstates and developmental stages, *Neuroimage* **16**(1) (2002) 41–48.
27. D. Lehmann, H. Ozaki and I. Pal, EEG alpha map series: Brain micro-states by space-oriented adaptive segmentation, *Electroencephalog. Clin. Neurophysiol.* **67**(3) (1987) 271–288.
28. D. Van de Ville, J. Britz and C. M. Michel, EEG microstate sequences in healthy humans at rest reveal scale-free dynamics, *Proc. Natl. Acad. Sci.* **107**(42) (2010) 18179–18184.
29. M. Ahmadlou and H. Adeli, Functional community analysis of brain: A new approach for EEG-based investigation of the brain pathology, *Neuroimage* **58**(2) (2011) 401–408.
30. K. Michalopoulos *et al.*, Classification of EEG single trial microstates using local global graphs and discrete hidden markov models, *Int. J. Neural Syst.* **26**(6) (2016) 1650036.

31. K. Michalopoulos and N. Bourbakis, Combining EEG microstates with fMRI structural features for modeling brain activity, *Int. J. Neural Syst.* **25**(8) (2015) 1550041.
32. M. Ahmadlou and H. Adeli, Visibility graph similarity: A new measure of generalized synchronization in coupled dynamic systems, *Physica D* **241**(4) (2012) 326–332.
33. M. Ahmadlou, H. Adeli and A. Adeli, Spatiotemporal analysis of relative convergence of EEGs reveals differences between brain dynamics of depressive women and men, *Clin. EEG Neurosci.* **44**(3) (2013) 175–181.
34. D. Rangaprakash, X. Hu and G. Deshpande, Phase synchronization in brain networks derived from correlation between probabilities of recurrences in functional MRI data, *Int. J. Neural Syst.* **23**(2) (2013) 1350003.
35. M. Ahmadlou, H. Adeli and A. Adeli, Improved visibility graph fractality with application for the diagnosis of autism spectrum disorder, *Physica A* **391**(20) (2012) 4720–4726.
36. E. A. Allen *et al.*, Tracking whole-brain connectivity dynamics in the resting state, *Cereb. Cortex* **24**(3) (2014) 663–676.
37. E. Damaraju *et al.*, Dynamic functional connectivity analysis reveals transient states of dysconnectivity in schizophrenia, *Neuroimage Clin.* **5** (2014) 298–308.
38. D. T. Jones *et al.*, Non-stationarity in the "Resting Brain's" modular architecture, *PLoS One* **7**(6) (2012) e39731.
39. A. Kucyi and K. D. Davis, Dynamic functional connectivity of the default mode network tracks daydreaming, *Neuroimage* **100** (2014) 471–480.
40. P. Barttfeld *et al.*, Signature of consciousness in the dynamics of resting-state brain activity, *Proc. Natl. Acad. Sci.* **112**(3) (2015) 887–892.
41. A. Elton and W. Gao, Task-related modulation of functional connectivity variability and its behavioral correlations, *Hum. Brain Mapp.* **36**(8) (2015) 3260–3272.
42. W. Boling *et al.*, Localization of hand motor activation in Broca's pli de passage moyen, *J. Neurosurg.* **91**(6) (1999) 903–910.
43. K. A. Pelphrey *et al.*, Functional anatomy of biological motion perception in posterior temporal cortex: An fMRI study of eye, mouth and hand movements, *Cereb. Cortex* **15**(12) (2005) 1866–1876.
44. B. Boroojerdi *et al.*, Localization of the motor hand area using transcranial magnetic stimulation and functional magnetic resonance imaging, *Clin. Neurophysiol.* **110**(4) (1999) 699–704.
45. R. Yupeng, P. Hyung-Soon and Z. Li-Qun, Developing a whole-arm exoskeleton robot with hand opening and closing mechanism for upper limb stroke rehabilitation, in *2009 IEEE Int. Conf. Rehabilitation Robotics. ICORR*, Kyoto, Japan (IEEE, 2009), pp. 761–765.
46. N. S. K. Ho *et al.*, An EMG-driven exoskeleton hand robotic training device on chronic stroke subjects: Task training system for stroke rehabilitation, in *2011 IEEE Int. Conf. Rehabilitation Robotics* (*ICORR*) (IEEE, 2011).
47. A. Ramos-Murguialday *et al.*, Brain–machine interface in chronic stroke rehabilitation: A controlled study, *Ann. Neurol.* **74**(1) (2013) 100–108.
48. S. J. Broyd *et al.*, Default-mode brain dysfunction in mental disorders: A systematic review, *Neurosci. Biobehav. Rev.* **33**(3) (2009) 279–296.
49. T. Yamanishi, J.-Q. Liu and H. Nishimura, Modeling fluctuations in default-mode brain network using a spiking neural network, *Int. J. Neural Syst.* **22**(4) (2012) 1250016.
50. C.-G. Yan and Y.-F. Zang, DPARSF: A MATLAB toolbox for "pipeline" data analysis of resting-state fMRI, *Front. Syst. Neurosci.* **4** (2010) 13.
51. J. Ashburner, A fast diffeomorphic image registration algorithm, *Neuroimage* **38**(1) (2007) 95–113.
52. K. J. Friston *et al.*, Movement-related effects in fMRI time-series, *Magn. Reson. Med.* **35**(3) (1996) 346–355.
53. J. D. Power *et al.*, Functional network organization of the human brain, *Neuron* **72**(4) (2011) 665–678.
54. S. P. Lloyd, Least squares quantization in PCM, *IEEE Trans. Inf. Theory* **28**(2) (1982) 129–137.
55. C. C. Aggarwal, A. Hinneburg and D. A. Keim, *On the Surprising Behavior of Distance Metrics in High-Dimensional Space*, J. Van den Bussche and V. Vianu (Eds.), ICDT 2001, LNCS 1973 (Springer, London, UK, 2001), pp. 420–434.
56. P. McCullagh, Generalized linear models, *Eur. J. Oper. Res.* **16**(3) (1984) 285–292.
57. R. B. O'hara and D. J. Kotze, Do not log-transform count data, *Methods Ecol. Evol.* **1**(2) (2010) 118–122.
58. W. Greene, Functional forms for the negative binomial model for count data, *Econ. Lett.* **99**(3) (2008) 585–590.
59. H. C. Chin and M. A. Quddus, Applying the random effect negative binomial model to examine traffic accident occurrence at signalized intersections, *Accid. Anal. Prev.* **35**(2) (2003) 253–259.
60. W. Gardner, E. P. Mulvey and E. C. Shaw, Regression analyses of counts and rates: Poisson, overdispersed Poisson, and negative binomial models, *Psychol. Bull.* **118**(3) (1995) 392.
61. A. M. Hermundstad *et al.*, Structural foundations of resting-state and task-based functional connectivity in the human brain, *Proc. Natl. Acad. Sci.* **110**(15) (2013) 6169–6174.
62. P. Delamillieure *et al.*, The resting state questionnaire: An introspective questionnaire for evaluation of inner experience during the conscious resting state, *Brain Res. Bull.* **81**(6) (2010) 565–573.
63. F. de Pasquale *et al.*, A cortical core for dynamic integration of functional networks in the resting human brain, *Neuron* **74**(4) (2012) 753–764.

64. S. Gu *et al.*, Controllability of structural brain networks, *Natl. Commun.* **6** (2015) 8414.
65. S. D. Keilholz, The neural basis of time-varying resting-state functional connectivity, *Brain Connect.* **4**(10) (2014) 769–779.
66. K. Christoff *et al.*, Experience sampling during fMRI reveals default network and executive system contributions to mind wandering, *Proc. Natl. Acad. Sci.* **106**(21) (2009) 8719–8724.
67. T. Chen *et al.*, Distinct global brain dynamics and spatiotemporal organization of the salience network, *PLos Biol.* **14**(6) (2016) e1002469.
68. F. I. Karahanoğlu and D. Van De Ville, Transient brain activity disentangles fMRI resting-state dynamics in terms of spatially and temporally overlapping networks, *Natl. Commun.* **6** (2015) 7751.
69. A. Shmuel and D. A. Leopold, Neuronal correlates of spontaneous fluctuations in fMRI signals in monkey visual cortex: Implications for functional connectivity at rest, *Hum. Brain Mapp.* **29**(7) (2008) 751–761.
70. Y. Nir *et al.*, Interhemispheric correlations of slow spontaneous neuronal fluctuations revealed in human sensory cortex, *Natl. Neurosci.* **11**(9) (2008) 1100–1108.
71. G. J. Thompson *et al.*, Neural correlates of time-varying functional connectivity in the rat, *Neuroimage* **83** (2013) 826–836.
72. M. D. Greicius *et al.*, Resting-state functional connectivity reflects structural connectivity in the default mode network, *Cereb. Cortex* **19**(1) (2009) 72–78.
73. M. P. van den Heuvel *et al.*, Functionally linked resting-state networks reflect the underlying structural connectivity architecture of the human brain, *Hum. Brain Mapp.* **30**(10) (2009) 3127–3141.
74. D. J. Hawellek *et al.*, Increased functional connectivity indicates the severity of cognitive impairment in multiple sclerosis, *Proc. Natl. Acad. Sci.* **108**(47) (2011) 19066–19071.
75. Y. I. Sheline *et al.*, Resting-state functional MRI in depression unmasks increased connectivity between networks via the dorsal nexus, *Proc. Natl. Acad. Sci.* **107**(24) (2010) 11020–11025.
76. N. U. Dosenbach *et al.*, Distinct brain networks for adaptive and stable task control in humans, *Proc. Natl. Acad. Sci.* **104**(26) (2007) 11073–11078.
77. E. Bullmore and O. Sporns, Complex brain networks: Graph theoretical analysis of structural and functional systems, *Natl. Rev. Neurosci.* **10**(3) (2009) 186–198.
78. D. S. Bassett and O. Sporns, Network neuroscience, *Natl. Neurosci.* **20**(3) (2017) 353–364.
79. D. A. Handwerker *et al.*, Periodic changes in fMRI connectivity, *Neuroimage* **63**(3) (2012) 1712–1719.
80. D. Prichard and J. Theiler, Generating surrogate data for time series with several simultaneously measured variables, *Phys. Rev. Lett.* **73**(7) (1994) 951.
81. J. Sun, X. Hong and S. Tong, Phase synchronization analysis of EEG signals: An evaluation based on surrogate tests, *IEEE Trans. Biomed. Eng.* **59**(8) (2012) 2254–2263.